



## Scalable purification of marennine and other exopolymers from diatom *Haslea ostrearia*'s “blue water”

William Bélanger<sup>a,b,\*</sup>, Richard Saint-Louis<sup>b</sup>, Bertrand Genard<sup>c</sup>, Jean-Sébastien Deschênes<sup>d</sup>, Réjean Tremblay<sup>a</sup>

<sup>a</sup> Institut des Sciences de la mer, Université du Québec à Rimouski, 310 des Ursulines, Rimouski, QC G5L 3A1, Canada

<sup>b</sup> Département de Biologie, Chimie et Géographie, Université du Québec à Rimouski, 300 des Ursulines, Rimouski, QC G5L 3A1, Canada

<sup>c</sup> Iso-BioKem, 300 des Ursulines, Rimouski, QC G5L 3A1, Canada

<sup>d</sup> Département de Mathématiques, Informatique et Génie, Université du Québec à Rimouski, 300 des Ursulines, Rimouski, QC G5L 3A1, Canada

### ARTICLE INFO

#### Keywords:

Exopolymers  
Solid-phase extraction  
Graphite  
Ionotropic gelation  
Diatom

### ABSTRACT

Marennine is a bioactive, polydisperse and polyanionic compound produced by certain benthic diatoms of the *Haslea* genus. Notably, *Haslea ostrearia* are cultivated in photobioreactors, and their supernatant is collected to extract extracellular marennine (EMn). EMn, a promising blue pigment, has several potential applications, including serving as a pathogenicity-reducing agent in the seafood industry. Nonetheless, its extraction and characterization remain challenging. To meet the need for an efficient, standardized and scalable preparative method, we introduce an improved route to concentrate and purify marennine, prioritizing cost-efficiency and process innocuity. As an exhaustive overhaul of our preliminary study for solid-phase extraction of EMn on synthetic graphitized carbon black, we revised every step to minimize solvent and reagents inputs, while enhancing the purity of the final products. Our improved solid-phase extraction (SPE) method employs natural graphite flakes as the stationary phase, from which the crude hydroorganic extract undergoes purification through ionotropic gelation, followed by chelator-assisted dissolution and cascade diafiltration. Extraction conditions are mild and maintain the ionization state of marennine throughout the process, also allowing for the reuse of both the stationary and the mobile phases. Upon optimization, the yield of the crude extract has been shown to reach up to 87 (6) %. The versatility of the novel process is further evidenced by the isolation of four distinct marennine groups, each with a different molecular weight, as well as four additional extracellular polymeric substances from the culture supernatant. Among these, the EMn fraction with a molecular weight range of 3–1 kDa achieved a mass absorptivity of 13.4 (0.6) L·cm<sup>-1</sup>·g<sup>-1</sup>, marking the highest level of purity reported thus far.

### 1. Introduction

Marennine is a bioactive halo- and electrochromic pigment [1,2] synthesized by marine diatoms of the genus *Haslea* [3,4]. It is a long-studied compound, still investigated for its growth inhibiting properties against pathogens belonging to the genus *Vibrio* [5–7]. As such, marennine could exert a prophylactic effect and mitigate pathogenicity factors of some bacteria [8] via a membrane stiffening mechanism, as shown for *Vibrio splendidus* [5]. Although its continuous culture remains a challenge [9], it is evolving from immobilized-cell photobioreactors (PBR) [10] to airlift cell suspensions, with optimization of culture

medium for *H. ostrearia* leading to enhanced biomass and marennine productivity [11]. Marennine accumulates in the apical regions of the cell before its release into the growth medium. Thus, it is not collected in the biomass, but in the supernatant of the PBR culture, commonly referred to as blue water (BW). As such, a novel harvesting method [12] improved on the design of submerged membrane PBR first proposed by Rossignol et al. [13], with the addition of polyvinylidene fluoride (PVDF) hollow fiber membranes permitting continuous cultivation without washout, resulting in higher cell density and marennine productivity.

Despite a great interest regarding marennine bioactivity and a rather

\* Corresponding author at: Institut des Sciences de la mer, Université du Québec à Rimouski, 310 des Ursulines, Rimouski, QC G5L 3A1, Canada.

E-mail addresses: [william.belanger2@uqar.ca](mailto:william.belanger2@uqar.ca) (W. Bélanger), [richard\\_st-louis@uqar.ca](mailto:richard_st-louis@uqar.ca) (R. Saint-Louis), [bertrand.genard@isobiokem.ca](mailto:bertrand.genard@isobiokem.ca) (B. Genard), [jean-sebastien.deschenes@uqar.ca](mailto:jean-sebastien.deschenes@uqar.ca) (J.-S. Deschênes), [rejean.tremblay@uqar.ca](mailto:rejean.tremblay@uqar.ca) (R. Tremblay).

<https://doi.org/10.1016/j.algal.2024.103879>

Received 20 August 2024; Received in revised form 18 December 2024; Accepted 19 December 2024

Available online 27 December 2024

2211-9264/© 2024 The Author(s). Published by Elsevier B.V. This is an open access article under the CC BY license (<http://creativecommons.org/licenses/by/4.0/>).

unique chromophore part of its molecular structure, its intricate chemical nature has yet to be fully described. Recent studies using nuclear magnetic resonance (NMR) have suggested a highly branched heteropolysaccharide bound to several aliphatic aglycons [3,14], but more work is needed. The challenges regarding its characterization arise in part from the complexity of marennine itself, being a large polymer with chromophore moieties, but also from limitations of current purification methods. Currently, the reference semipreparative process uses ultrafiltration (30–3 kDa), followed by anion-exchange chromatography and dialysis [15]. However, important drawbacks of this approach can be problematic for commercial applications. Specifically, analyte concentration through ultrafiltration of large BW volume is slow, and the appropriate membrane sizes can be challenging to source at certain scales. Likewise, despite providing high purification, chromatography is typically expensive due to its low throughput and the complexity involved in scaling up [16].

In order to solve those issues, we propose the first preparative, scalable method. From recent insights regarding interactions between marennine and carbonaceous sorbents [17], we optimized the solid-phase extraction (SPE) step by replacing both the stationary and mobile phases, which now use graphite in replacement of graphitized carbon black (GCB), along with a simple water-butanone mixture as the eluent. Those changes are expected to minimize undesirable ionic interactions and prevent the need for chemical additives such as reductants and buffers. With those improvements, we suggest using our inexpensive SPE extraction to concentrate the bulk BW upstream and thus minimize the ultrafiltration volume. In replacement of chromatography, the crude extract obtained from SPE can be selectively gelled, which isolates marennine from co-eluted compounds sharing similar properties. Our improved method thus achieves similar quality to anionic chromatography, with minimal specialized equipment, while valorizing newly discovered co-extracted compounds mostly composed of sulfated polysaccharides with commercial potential.

The use of a single, low-boiling point solvent in the SPE eluent opens the possibility to further improve environmental performance by facilitating recycling with low-cost technologies such as rotary evaporation. Likewise, ionotropic gelation, a selective precipitation method, prevents

the need for large volumes of ethanol and replaces previous halogenated chemicals, dichloromethane and trifluoroacetic acid, with calcium and phosphate salts. A straightforward and cost-effective route for marennine extraction is thus proposed in this paper. Carefully chosen green inputs are used to ensure efficiency, safety, and preservation of marennine integrity. Additionally, stationary phase reconditioning is demonstrated through a simple heat treatment, further reducing costs. As a result, the process now aligns with five green chemistry principles: waste prevention, use of safe solvents and auxiliaries, use of renewable feedstocks, energy-efficient design, and safer chemistry for accident prevention.

Although marennine is typically considered to fall within the 10 kDa range [2], we fractionated it into four distinct molecular weight classes: high (HMW), medium (MMW), low (LMW), and very low molecular weights (VLMW), ranging from over 30 kDa to under 1 kDa. Altogether, the fractionation process yields eight compounds, four of which are sulfated polysaccharides devoid of marennine chromophore. These advances are a valuable asset for future research on the characterization of marennine molecules and the valorization of *Haslea ostrearia* culture.

## 2. Material and method

The Fig. 1 presents the workflow of the novel extraction process. The purification previously achieved during pre-elution wash and ethanol precipitation [17] now occurs concurrently with the ionotropic gelation. Marennine-containing BW was produced in five 30 L flat-bottom PBRs, as described in Prasetya et al. [10].

### 2.1. Solid-phase extraction improvements

#### 2.1.1. Cartridges preparation, elution and quantification method

The cartridges used in this section were prepared using 100 mg of graphite flakes, –325 mesh (50–70 %), ≥99% carbon (Sigma-Aldrich, Oakville, Canada), dry-loaded between two fritted glass fiber discs into polypropylene syringes (1 mL volume, 5.6 mm inner diameter). The sorbent was then packed with a glass rod to reach a height of 7.1 mm in between discs, for a final volume to mass ratio of 1.75 mm<sup>3</sup>·mg<sup>-1</sup>.

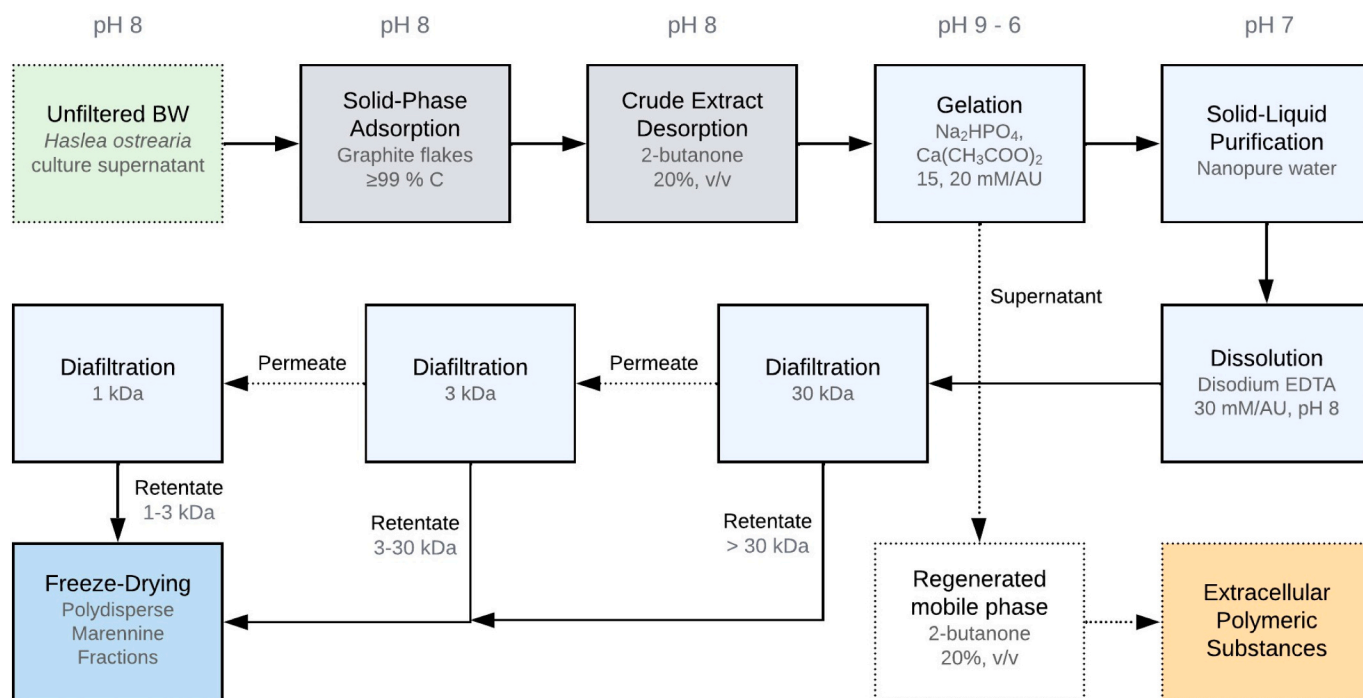


**Fig. 1.** Process flow diagram of the improved extraction process using graphite-based solid-phase extraction and calcium phosphate ionotropic gelation. Following hydrogel dissolution in ethylenediamine tetraacetate (EDTA), marennine polymers are purified and optionally fractionated by cascade diafiltration.

Marennine crude extracts (CE) were eluted using a mobile phase of dilute 2-butanone in either water or aqueous buffer, followed by an aqueous rinse to thoroughly drain the remaining eluent. Both fractions were collected directly into graduated glass conical tubes and gauged with water at a fixed volume prior to UV–Visible (UV–Vis) analysis. The concentration of marennine was determined at 22 °C using an Agilent Cary 100 spectrophotometer (Santa Clara, CA, USA) with Varian WinUV software (version 3.00), with a scan rate of 600 nm·min<sup>-1</sup> and 1 nm interval. Marennine concentration is assessed based on its absorbance at the  $\lambda_{\text{max}}$  wavelength between 560 and 800 nm. Since the absorbance maxima of marennine can slightly vary depending on its chemical environment, the unit  $A_{\text{max}}$  refers to the maximum absorbance at this wavelength range. Unless stated otherwise, samples absorbance was recorded using a quartz microcuvette with a path length of 1 cm.

### 2.1.2. Eluent concentration

In quintuplicate, cartridges were loaded with 25 mL BW (0.04  $A_{657 \text{ nm}}$ ) and eluted using 600  $\mu\text{L}$  of aqueous sodium phosphate buffer (5 mM, pH 8), with butanone concentration ranging from 0 to 20 % (v/v). The eluent was rinsed using 1200  $\mu\text{L}$  of deionized water (DW) and gauged at 2 mL with DW. The highest concentration was set to 20 % to ensure complete solubility of butanone in water.

### 2.1.3. Graphite conditioning and backflush desorption

In quintuplicate, the conditioned sorbents were prepared by adding 600  $\mu\text{L}$  of methanol followed by 600  $\mu\text{L}$  of a 50 mM sodium phosphate buffer (pH 8). These samples were then loaded with 5.1 mL BW (0.10  $A_{658 \text{ nm}}$ ) and the stationary phase was kept wet at all times. For the backflush and control groups, the cartridges were loaded with 5.1 mL BW, with the cartridges turned upside-down prior to elution for the backflush group, as recommended by Hennion [18] for carbonaceous sorbents. All samples were eluted with 600  $\mu\text{L}$  of a 2:8 (v/v) mixture of butanone and water, rinsed with 600  $\mu\text{L}$  DW and gauged at 1.5 mL.

### 2.1.4. Reductants effect on desorption for graphite and GCB

In quintuplicate, the reduced graphite and GCB sorbents were prepared by conditioning the stationary phase with 600  $\mu\text{L}$  of 60 mM sodium metabisulfite followed by 600  $\mu\text{L}$  of DW, whereas the control groups were only rinsed with 1200  $\mu\text{L}$  of deionized water (DW). The graphite and GCB cartridges were then loaded with 5.1 and 89 mL of BW (0.10  $A_{658 \text{ nm}}$ ), respectively. The crude extracts were eluted with 600  $\mu\text{L}$  of a 2:8 (v/v) mixture of butanone and water, with the addition of 5 mM sodium sulfite for the reduced groups, followed with 600  $\mu\text{L}$  of DW. The eluates from the graphite cartridges were gauged at 1.5 mL, whereas those from GCB were gauged at 3 mL.

### 2.1.5. Graphite regeneration

**2.1.5.1. Effect of heat treatment on crude marennine yield.** The evolution of yield to waste proportion was monitored during successive extractions. In triplicate, cartridges containing 125 mg of graphite (–325 mesh) were loaded with 30 mL of BW (0.06  $A_{660 \text{ nm}}$ ), then eluted with a 2:8 (v/v, 750  $\mu\text{L}$ ) mixture of butanone and sodium phosphate buffer (5 mM, pH 8), followed by 1 mL water wash and volume gauging to 2 mL. Following five consecutive extractions, the graphite was pushed out of the cartridge and regenerated by heating at 400 °C for 6 h. The regeneration-load-elution cycle was repeated twice, totaling 3 rounds of 5 extractions using the same sorbent. Waste was collected during the loading phase, then its UV–Visible absorbance was analyzed with a quartz cuvette of 10 cm path length. Crude extract absorbance was recorded using a quartz microcuvette of 1 cm path length.

**2.1.5.2. Thermogravimetric analysis.** In duplicate, spent graphite was prepared by performing three successive BW adsorption and desorption sequences onto the same stationary phase. Briefly, for each group two

cartridges of 1 mL volume were filled with 100 mg graphite (–325 mesh), then loaded with 18 mL of BW (0.09  $A_{661 \text{ nm}}$ ) and eluted with aqueous butanone (20 %, v/v) followed by 1.2 mL of nanopure water (NW). Regenerated graphite samples were heated at 400 °C during 6 h beforehand, whereas blanks were prepared by using pristine graphite and NW in replacement of BW. The samples were then analyzed in a thermogravimetric analyzer from Perkin Elmer, model TGA 8000 (Shelton, CT, USA), from 60 to 1000 °C at a rate of 15 °C·min<sup>-1</sup>, with a 15 min hold at 400 °C.

### 2.1.6. Marennine adsorption isotherm for graphite and GCB

**2.1.6.1. Adsorption isotherm determination.** Three types of natural graphite flakes were compared for their adsorption capabilities. From finer to coarser, the particle sizes were –325 mesh (50–70 %), –100 mesh ( $\geq 80\%$ ) and +50 mesh ( $\geq 80\%$ ). In duplicate, an increasing mass of graphite was weighted into 50 mL polypropylene conical centrifugation tubes, followed by the addition of 35 mL of BW (0.93  $A_{660 \text{ nm}}$ , 10 cm). The tubes were mixed by vortex followed by 30 min ultrasonication at 22 °C, in order to reach adsorption equilibrium. Samples were then centrifuged (4000 g, 15 min) and the supernatant filtered on a 0.45  $\mu\text{m}$ , 25 mm syringe-mounted nylon disc (VWR, Radnor, PA, USA). UV–Vis absorbance was measured using a quartz cuvette of 10 cm path length, with centrifuged BW as the control group. The same procedure was repeated using GCB and heat-treated graphite (400 °C, 6 h), with 0.94  $A_{661 \text{ nm}}$  (10 cm) and 1.45  $A_{659 \text{ nm}}$  (10 cm) BW, respectively.

**2.1.6.2. Crude extract yield at near saturation.** In quintuplicate, 100 mg 1 mL cartridges were prepared for both –325 mesh and –100 mesh graphite, with and without heat treatment (400 °C, 6 h), as well as five 3 mL cartridges containing 1 g of +50 mesh graphite and five commercial 100 mg GCB cartridges. These columns were loaded with BW (0.09  $A_{672 \text{ nm}}$ ) at 90 % marennine saturation in accordance with adsorption isotherm results for each sorbent. CE elution was carried out using 1.8 mL of aqueous butanone solution (20 %, v/v) into 15 mL glass graduated tubes, followed by 900  $\mu\text{L}$  of DW rinse and gauged to 3 mL before UV–Vis analysis. In order to maximize contact duration, both the BW and the eluent were added at a very slow pace, below 1 drop·s<sup>-1</sup>.

### 2.1.7. Raman as a prediction tool of ionic interactions

Graphite samples were analyzed by a DXR Raman Microscope (Thermo Fisher Scientific, Waltham, MA, USA), equipped with a full range diffraction grating of 900 lines·mm<sup>-1</sup> and a 532 nm green laser (diode-pumped, solid state) over a wavenumber range of 180 to 3500 cm<sup>-1</sup>. Laser power was set to 10 mW, and the spectra were recorded using 64 scans and a collection exposure of 1 s with a 50  $\mu\text{m}$  slit aperture, using a MPlan 50 $\times$  magnification objective. The spectra were acquired with OMNIC for dispersive Raman software (9.2.387) and recorded in five random locations, spanned over 9 points on a surface of 16  $\times$  16  $\mu\text{m}$  with a step size of 8  $\mu\text{m}$ , totaling 45 acquisitions per sample. Spectra were normalized according to the G peak intensity near 1575 cm<sup>-1</sup>. Normalization and mean value calculation were done using Spectragryph optical spectroscopy software (1.2.15).

### 2.1.8. Sedimentation time optimization for batch extraction

Optimal duration of sedimentation was determined by gravimetric analysis. Briefly, in quintuplicate, 10 g of graphite (–325 and –100 mesh) was mixed into 1 L of DW at 22 °C, and the supernatant was sampled after a delay ranging from 15 min to 4 h. The supernatant was filtered onto dried GF/F 2.5 cm glass microfiber filters (Ahlstrom-Munksjö, Kaukauna, US), dried 24 h at 100 °C and weighted to determine the mass of particulate matter.

## 2.2. Reversible ionotropic gelation

The efficacy of ionotropic gelation relies on the precise concentration balance between marennine concentration, calcium and phosphate ions. These parameters are thoroughly examined in the subsequent experiments.

### 2.2.1. Gelation (sol-gel transition)

Optimal calcium and hydrogen phosphate concentrations were determined following a two-part experiment. Initially, marennine from the hydroorganic crude extract (butanone 20 %, v/v) was gelified with either calcium acetate alone, or with equimolar addition of disodium phosphate and calcium acetate at 22 °C, using both dilute (0.91 A<sub>655 nm</sub>) and concentrated (2.85 A<sub>663 nm</sub>) extracts. In triplicate, 50 µL of DW or concentrated disodium phosphate solution were added into 700 µL of CE, then mixed with 50 µL of calcium acetate to reach concentration ranging from 0 to 25 mM·A<sub>max</sub><sup>-1</sup>. The samples were left 10 min to gelify then centrifuged at 20,000 g during 5 min. The absorbance of the supernatant was measured to determine marennine concentration.

According to the optimal calcium concentration determined previously, in triplicate, 50 µL of concentrated disodium phosphate solution were mixed into 700 µL of CE (1.04 A<sub>659 nm</sub>) to reach concentration between 1 and 60 mM·A<sub>max</sub><sup>-1</sup>, then 50 µL of calcium acetate were added for a fixed concentration of 20 mM·A<sub>max</sub><sup>-1</sup>. The samples were left 10 min to gelify then centrifuged at 20,000 g during 5 min. The controls were prepared by adding DW instead of phosphate and calcium solutions. The absorbance of the supernatant was measured to determine marennine concentration. Lastly, the supernatant of each triplicate were combined to measure their hydroorganic pH using an Accumet basic AB15 meter with a standard pH combination electrode, model 13-620-287a (Thermo Fisher Scientific, Waltham, MA, USA).

### 2.2.2. Dissolution (gel-sol transition)

In triplicate, 700 µL of CE (0.91 A<sub>655 nm</sub>) was added into 1.5 mL microcentrifuge tubes and mixed with 50 µL disodium phosphate, then 50 µL calcium acetate to reach 20 mM·A<sub>max</sub><sup>-1</sup> of each. The samples were left to gelify for 10 min at 22 °C then centrifuged at 20,000 g during 5 min. The supernatant was discarded and the remaining hydrogel was dissolved into 700 µL of aqueous EDTA solution (0–35 mM·A<sub>max</sub><sup>-1</sup>) or glutamate diacetate (L-GLDA, 0–70 mM·A<sub>max</sub><sup>-1</sup>) adjusted to pH 8.00. The marennine pellets were dislodged with 3 cycles of 10 min vortex mixing (3000 RPM, 10:1 s on/off pulses) followed by 10 min ultrasonication at 22 °C, until a complete dissolution or an even suspension was achieved. The tubes were centrifuged once more and the absorbance of the supernatant was measured to determine marennine concentration. The resolubilization yield was established according to the absorbance of the control groups, which were prepared by centrifugation of the CE without further additions. Lastly, five more pellets were prepared in the same manner then dried at 100 °C overnight to determine the residual mass of solvent in the hydrogel.

## 2.3. Scaled extraction and purification

### 2.3.1. Solid-phase extraction

24 L of unfiltered BW (0.08 A<sub>659 nm</sub>) was pumped into a conical tank equipped with a removable bottom container (FermZilla Tri-Clover, KegLand, Noble Park North, Victoria, Australia). Marennine was extracted by 15 min overhead mechanical agitation of graphite (382 g, -325 mesh) in BW, after which the marennine-loaded graphite was recovered by detaching the collection vessel following a 2 h sedimentation period. In addition, a sequential extraction was performed to recover more extracellular polymeric substances (EPS) from the same BW, by adding 700 g of +50 mesh graphite, followed by 15 min agitation and 30 min sedimentation. Successively, the sorbents were added into a fritted 53 mm diameter by 254 mm chromatographic column

(Synthware, Pleasant Prairie, WI, USA) layered with filtration quartz media (0.45–0.55 mm). For the -325 mesh graphite, marennine was eluted with 1.5 L of 20 % (v/v) aqueous butanone and the column output was connected to a SPE manifold to collect the crude extract into volumes ranging from 10 mL to 50 mL. For each fractions, 200 µL aliquots were then placed in a 96-well plate for elution profile determination using an Agilent Synergy H1 microplate reader (Mississauga, ON, Canada). All those crude extract samples were then combined and filtered twice on a 47 mm GF/F (Whatman, Buckinghamshire, UK) prior to absorbance analysis in a quartz microcuvette with 1 cm path length, using a Cary 100 spectrophotometer (Agilent, Santa Clara, CA, USA). The +50 mesh graphite was eluted using 1 L of 20 % (v/v) aqueous butanone and filtered twice on a 47 mm GF/F. The workflow of the sequential extraction is depicted in Fig. 2.

### 2.3.2. Reversible ionotropic gelation

Marennine crude extract (1.5 L, 0.86 A<sub>658 nm</sub>) was gelified with the addition of disodium phosphate (15 mM·A<sub>max</sub><sup>-1</sup>) and calcium acetate (20 mM·A<sub>max</sub><sup>-1</sup>) at 22 °C. The samples were mixed and left 30 min to gelify, then centrifuged at 5000g during 15 min (Beckman Coulter Avanti J-E, rotor JLA-9.1000) and the supernatant was reserved. Thrice, the gel was suspended into 1 L of NW using a magnetic stir plate, then centrifuged again. Lastly, the washed marennine hydrogel was mixed into aqueous EDTA solution (pH 8, 30 mM·A<sub>max</sub><sup>-1</sup>) until complete dissolution was achieved. The resulting aqueous extract was filtered twice on GF/F 47 mm (Whatman, Buckinghamshire, UK).

### 2.3.3. Cascade diafiltration

In order to remove contaminants and to isolate marennine fractions by their molecular weight, the resolubilized extracts were purified by cascade diafiltration using a 400 mL Amicon stirred cell apparatus with 76 mm regenerated cellulose membranes (MilliporeSigma, Oakville, ON, Canada), fitted to a 19 L Cornelius ball lock keg reservoir (Amcyl, Wyoming, MN, USA) filled with NW and pressurized with nitrogen at 50 psi. For each successive molecular weight cut-offs, at 30, 3 and 1 kDa, the sample was first concentrated down to roughly 50 mL using gas pressure (batch concentration mode), then purified in continuous mode with NW until the permeate reached a conductivity below 10 µS·cm<sup>-1</sup> (Oakton EcoTestr EC1, Environmental Express, Charleston, SC, USA). Sequentially, the collected permeates were filtrated onto narrower membrane and the retentates were freeze-dried, yielding three purified marennine fractions. To remove remaining culture dirt and debris prior to freeze-drying, the 30 kDa retentate was filtrated on a 2.5 cm GF/F glass microfiber filter (Ahlstrom-Munksjö, Kaukauna, US), followed by filtration on a 25 mm 0.45 µm syringe-mounted nylon disc (VWR, Radnor, PA, USA). Salt residues were approximated according to the electrical conductivity (EC) of each fraction, using an Oakton EcoTestr EC1 conductivity meter. Assuming NaCl as the dominant species, the EC values (µS·cm<sup>-1</sup>) were multiplied by a factor of 0.64 [19].

### 2.3.4. End-permeate valorization

In addition to the collected retentates, with class of compounds with molecular weight ranges of 3–1 kDa, 30–3 kDa, and >30 kDa, very low molecular weight marennine (VLMW, <1 kDa) was recovered from the end process permeate. As such, a second SPE was performed to eliminate EDTA complexes and other side products (Fig. 3). Briefly, 70 g of graphite (-325 mesh) was mixed into roughly 40 L of DW containing 7.2 L of 1 kDa permeate (0.3748 A<sub>673 nm</sub>, 10 cm) for 15 min. The graphite was left to settle for about 48 h then poured onto layers of diatomaceous earth and filtration quartz into a fritted flash chromatography column. Yellow contaminants were rinsed off with DW until the column output became clear, then the VLMW marennine fraction was eluted with 300 mL of aqueous butanone solution (20 %, v/v) and filtered twice on 47 mm GF/F (Whatman, Buckinghamshire, UK). The filtrate was dried using a rotary evaporator (35 °C, < 25 mbar) and resolubilized in a minimal volume of NW, then filtrated on a 0.45 µm, 25 mm syringe-

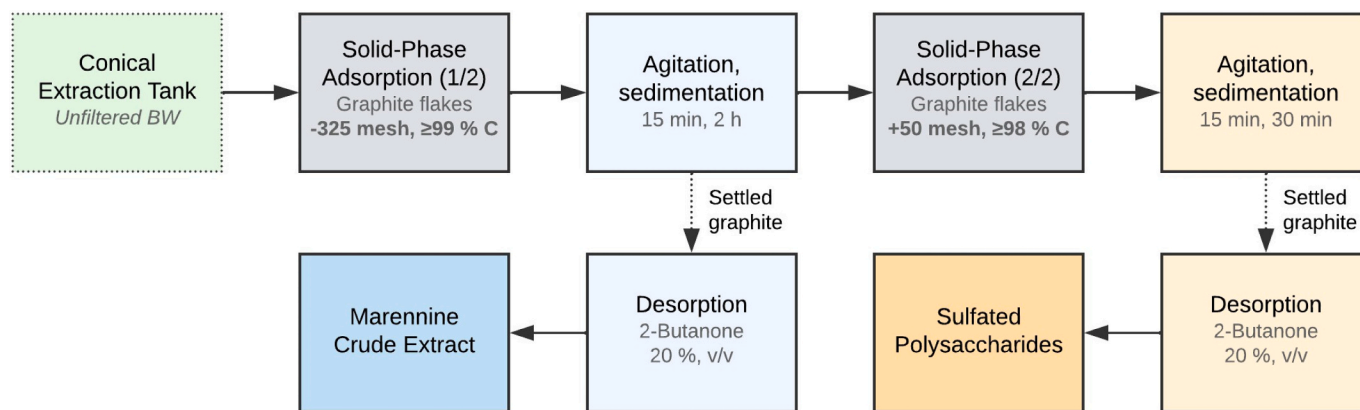


Fig. 2. Process flow diagram of the scaled sequential extraction of exopolymers from *Haslea ostrearia* culture supernatant (BW), using two successive solid-phase extractions (SPE) with different types of graphite on the same BW batch.

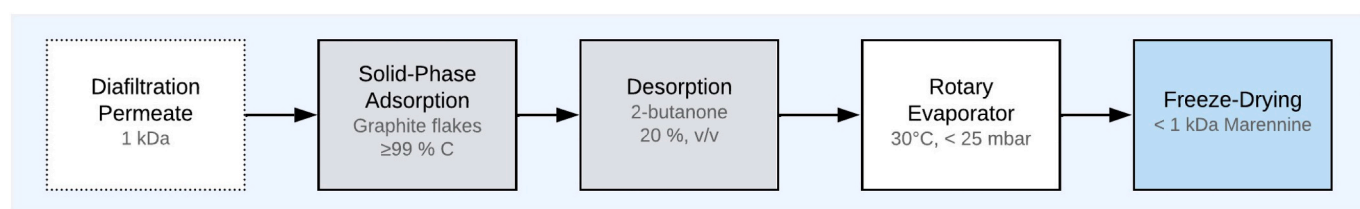


Fig. 3. Process flow diagram for the extraction of very low molecular weight marennine (<1 kDa) from the 1 kDa diafiltration permeate.

mounted nylon disc (VWR, Radnor, PA, USA) and freeze-dried.

### 2.3.5. Cation-induced spectral shift

In order to assess the relationship between salinity and changes in absorbance intensity of the marennine chromophore, diafiltrated medium molecular weight marennine (MMW, 30–3 kDa retentate) was subjected to a progressive addition of cations to assess the resulting spectral shifts. As such, an aqueous marennine solution was mixed with sodium and magnesium chloride to reach final concentrations of  $0.1 \text{ g}\cdot\text{L}^{-1}$  marennine and about 50 to 500 mM of each salt. The microplate was mixed for 60 s and the absorbance was measured immediately at  $25^\circ\text{C}$  with an Agilent Synergy H1 (Mississauga, ON, Canada).

### 2.3.6. Mass absorptivity

In triplicate, freeze-dried samples of purified marennine were weighted on a microbalance Cubis 3.6P-2500-M (Sartorius, Goettingen, Germany) and dissolved in sodium phosphate buffer (10 mM, pH 8).

### 2.3.7. EPS extraction and characterization

**2.3.7.1. EPS extraction.** The extraction of EPS from BW can be achieved via either sequential SPE (Fig. 2), or through marennine co-extraction (Fig. 4). After marennine gelation, the supernatant was dried via rotary evaporation ( $40^\circ\text{C}$ , < 25 mbar), dissolved in a minimal volume of dilute HCl (30 mM) and neutralized with equimolar NaOH addition. In comparison, EPS from sequential extraction were only concentrated near dryness by rotary evaporation. Both samples were filtered through a #2 cellulose filter (Whatman, Buckinghamshire, UK), and concentrated to roughly 50 mL on a 1 kDa diafiltration membrane, then diafiltrated in continuous mode until the permeate reached a conductivity below  $10 \mu\text{S}\cdot\text{cm}^{-1}$  (Oakton EcoTestr EC1). The purified EPS mixtures were freeze-dried then washed five times with methanol to yield lipophobic (EPS-H<sub>2</sub>O) and methanol-soluble (EPS-MeOH) fractions. Salt residues were approximated according to the EC of each sample, using an Oakton EcoTestr EC1 conductivity meter with a conversion factor of

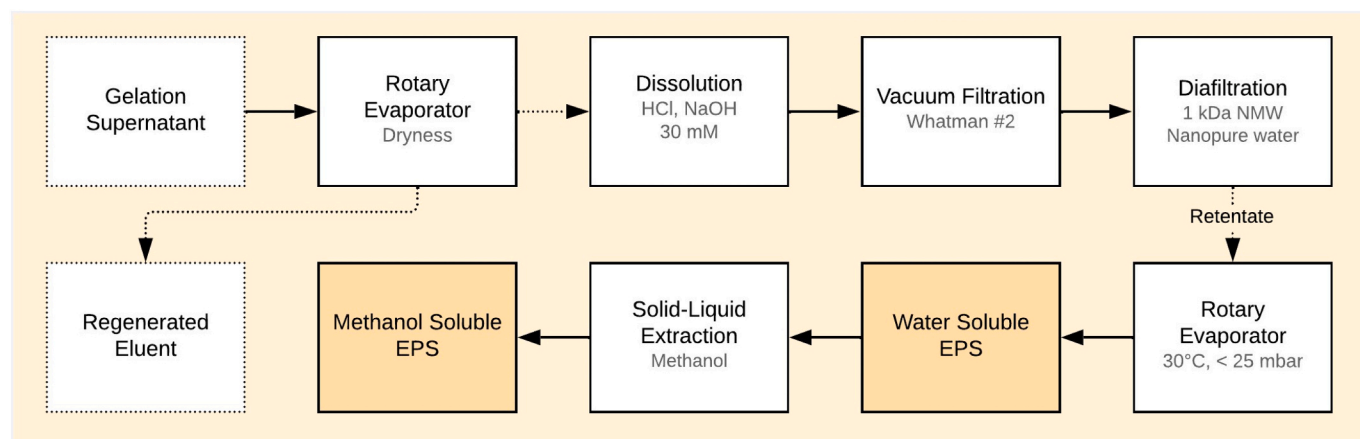


Fig. 4. Process flow diagram for extracellular polymeric substances (EPS) recovery and purification from the ionotropic gelation supernatant.

0.64.

**2.3.7.2. Fourier Transform Infrared Spectroscopy (FTIR).** The Nicolet iS10 FTIR spectrometer equipped with a Smart iTR diamond Attenuated Total Reflection (ATR) module (Waltham, MA, USA) was used to analyze the freeze-dried samples. With OMNIC software (7.3), spectra were collected between 525 and 4000  $\text{cm}^{-1}$ , with a gain of 1.0, a medium resolution aperture, and 128 scans per sample. Commercial fucoidan extracted from *Fucus vesiculosus* was used as the standard. Spectra processing was done with Spectragryph optical spectroscopy software (1.2.15).

**2.3.7.3. Sulfated polysaccharides determination.** As described in Hahn et al. [20], the cationic dye toluidine blue was used to selectively determine sulfated polysaccharides. The experiment was conducted at acidic pH to ensure protonation of the anionic groups of interfering compounds, such as phosphorylated and carboxylated polymers, which have higher pKa values compared to sulfate esters. Briefly, a toluidine blue solution (0.05 mM) was prepared into a HCl-KCl buffer (20 mM, pH 1) and mixed with aqueous analyte samples of concentration ranging from 0.5 to 50  $\mu\text{g}\cdot\text{mL}^{-1}$ . As such, 275  $\mu\text{L}$  of reagent was mixed for 60 s with 25  $\mu\text{L}$  of each analyte, and the absorbance was measured immediately at 25 °C with Agilent Synergy H1 microplate reader (Mississauga, ON, Canada). Slopes were calculated by plotting sample concentration with absorbance attenuation at 632 nm. In addition to fucoidan and the four EPS samples, MMW marennine was also analyzed.

## 2.4. Reagents

Most reagents were sourced from Sigma-Aldrich (Oakville, ON, Canada), including graphite (-325, -100 and +50 mesh), GCB cartridges (100 mg, Supelco EnviCarb), 2-butanone ( $\geq 99.7\%$ ), disodium phosphate heptahydrate ( $\geq 98\%$ ), calcium acetate monohydrate ( $\geq 99.0\%$ ), anhydrous magnesium sulfate ( $\geq 99.5\%$ ), methanol ( $\geq 99.9\%$ ), trifluoroacetic acid ( $\geq 99.9\%$ ), sodium chloride ( $\geq 99.5\%$ ), magnesium chloride hexahydrate ( $\geq 99.0\%$ ) and fucoidan ( $\geq 95\%$ ). Dichloromethane ( $\geq 99.9\%$ ) and tetrasodium L-GLDA were bought from Fisher Scientific (Fair Lawn, NJ, US) and ethanol (USP grade) from Greenfield Global (Boucherville, QC, Canada). Acetonitrile ( $\geq 99.9\%$ ) was sourced from Canadian Life Science (Vaureuil-Dorion, QC, Canada) and tetrasodium EDTA ( $\geq 99.5\%$ ) from VWR (Edmonton, AB, Canada). Toluidine blue (58 %) was bought from JT Baker Chemical (Philipsburg, NJ, USA).

## 2.5. Statistical analysis

Normality and homoscedasticity were assessed using Shapiro–Wilk and Leneve's test, respectively. When the null hypothesis of a normal distribution could not be rejected for all treatment groups, parametric tests were used to validate differences between treatments, using an analysis of variance (ANOVA), followed by a post hoc Tukey HSD test. Else, the differences were assessed with Kruskal–Wallis and Wilcoxon rank-sum tests. Data are expressed as means value ( $\pm$ standard deviation), and the statistical analysis done with R software (version 4.2.0–4) with packages agricolae (1.3–5), car (3.0–13), multcompView (0.1–8) and rcompanion (2.4.15). An alpha value of 0.05 was considered significant for all statistical analysis.

## 3. Results

Several changes were implemented to improve the solid-phase extraction and the purification process. The stationary and mobile phases were optimized for marennine extraction, while anti-solvent precipitation and pre-elution wash were substituted with in situ synthesis of calcium phosphate salts using disodium phosphate and calcium acetate, a selective gelation method for marennine. The key

improvements are outlined in Table 3.

### 3.1. Solid-phase extraction improvements

#### 3.1.1. Eluent concentration

The buffered mobile phase achieved 23 (4) % yield in absence of organic modifier, while the CE yield increased as the concentration of butanone rose up. The average yield reached 59 (3) % at the highest butanone concentration (fig. S1).

#### 3.1.2. Graphite conditioning and backflush desorption

Superior marennine recovery, reaching 84 (2) %, was achieved with backflush desorption. In average, yield attained 72 (7) % in the conditioned and control groups (fig. S2), which were not significantly different.

#### 3.1.3. Reductants effect on desorption for graphite and GCB

The addition of sodium metabisulfite and sodium sulfite to the stationary phase and eluent, respectively, had a significant effect on the desorption of marennine from EnviCarb GCB, whereas there was no improvement in yield observed for natural graphite flakes (fig. S3).

#### 3.1.4. Graphite regeneration

For each round of five successive extractions, the yield to waste ratio decreased progressively in a reverse power trend ( $R^2 = 0.9887$ ), whose decline was reset by a simple heat treatment (fig. S4). Statistical analysis revealed no significant differences for the yield and waste outputs of the two initial extractions, suggesting that the sorbent can be successfully used twice between heat treatments, with moderate losses (table S1). An average yield of 60 (3) % was achieved for those two extractions, as the sorbent was oversaturated. The total output, resulting from the addition of marennine found in yield and waste, was always  $<100\%$  (fig. S5). This suggests a possible capping mechanism onto polar groups of graphite surface, and may explain why the yield is slightly higher for the second extraction among the heat-treated samples.

#### 3.1.5. Marennine adsorption isotherm for graphite and GCB

The adsorption capacity at equilibrium ( $Q_e$ ) of different types of graphite were investigated, with -325 mesh graphite showing slightly better performance than -100 mesh and significantly higher capacity than +50 mesh graphite (fig. S8). Strikingly, the adsorption capacity of GCB was found to be roughly ten times higher than the best graphite (fig. S9). The results from the adsorption isotherms (fig. S10) and successive extraction experiment (fig. S4) suggest that heat treatment enhances the adsorption capacity of graphite. This is further supported by thermogravimetric analysis which showed a lower mass loss for heat-treated graphite compared to pristine graphite (fig. S7). Table S2 presents the  $Q_e$  values enabling near 100 % marennine uptake, along with the yield of each stationary phase at 90 % saturation. Eq. (1) describes the mass of graphite required to adsorb dissolved marennine from the BW, where the variable  $A_{\text{max}}$  indicates the absorbance at the  $\lambda_{\text{max}}$  between 620 and 700 nm,  $V$  is the BW volume and  $l$  is the cuvette path length.

$$m_{\text{graphite}}[\text{g}] = \frac{A_{\text{max}}[\text{AU}] \cdot V[\text{L}]}{Q_e[\text{AU} \cdot \text{L} \cdot \text{g}^{-1} \cdot \text{cm}^{-1}] \cdot l[\text{cm}]} \quad (1)$$

#### 3.1.6. Raman as a prediction tool of ionic interactions

The Raman spectra of graphite and GCB show the typical carbon-hydrogen stretching bands ascribed to  $\text{sp}^3$  defects (D), planar  $\text{sp}^2$  carbon atoms (G) and the thickness of graphene layers (2D) [21]. The relative intensities of these peaks in graphite are notably different from those of GCB (Fig. S11). In particular, the  $I_D/I_G$  ratio of GCB is about twenty times higher than -325 mesh graphite, while its  $I_{2D}/I_G$  ratio is twice higher. Further information on Raman data of GCB and graphite is detailed in table S3, while Fig. 5 presents the relationship between  $I_D/I_G$  ratios and crude extract yield results discussed in Section 3.1.5.

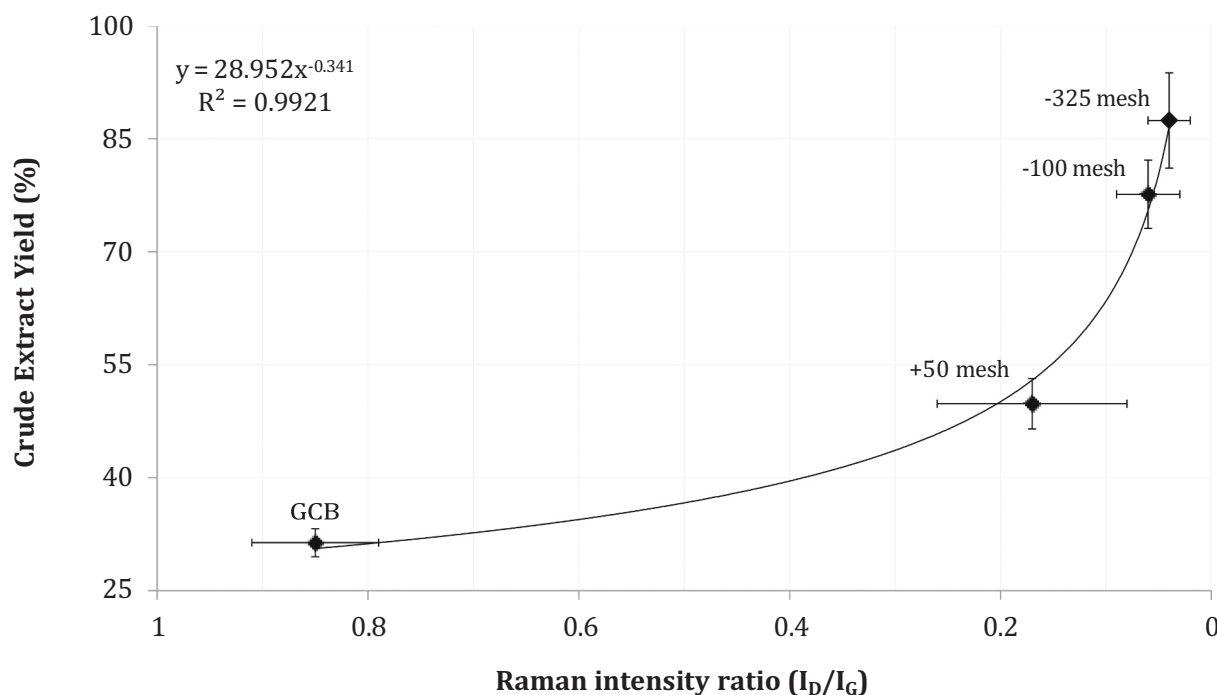


Fig. 5. Relationship of marennine SPE crude extract yield at 90 % saturation and the  $I_D/I_G$  Raman bands ratio for GCB and three graphite samples.

### 3.1.7. Sedimentation time optimization for batch extraction

The results of the gravimetric analysis demonstrate that after one hour of sedimentation, nearly all graphite particles had settled out. Specifically, roughly 0.10 and 0.15 % of particles remained in suspension for the –100 and –325 mesh samples (fig. S12). As anticipated, due to its coarser particle size, –100 mesh graphite was found to settle faster than –325 mesh. While almost complete sedimentation occurred after 5 h, some very fine particulate remained suspended beyond this time and thus could not be recovered.

## 3.2. Reversible ionotropic gelation

### 3.2.1. Gelation (sol-gel transition)

The addition of calcium and phosphate ions to the CE caused a near-instantaneous gelation of marennine, which after centrifugation left a dark green pellet and a pale yellow supernatant. With phosphate-containing extracts, marennine gelation reached a plateau near 15  $\text{mM}\cdot\text{AU}^{-1}$ , and a maximum at 20  $\text{mM}\cdot\text{AU}^{-1}$  where the chromophore could no longer be detected in the supernatant (fig. S13). The maximum gelation achieved was 100 (0) % in concentrated CE and 99 (0) % for the diluted extract. When hydrogen phosphate was removed, however, the gelation only reached 29 (2) % at the highest calcium concentration tested. According to these results, Eq. (2) can be used to determine the required calcium concentration to completely gelify marennine in dilute butanone extracts (pH 8, 20 % butanone,  $v/v$ ).

$$[\text{Ca}^{2+}] = A_{\max} [\text{AU}] \cdot l [\text{cm}] \cdot 20 \left[ \text{mM} \cdot (\text{AU} \cdot \text{cm})^{-1} \right] \quad (2)$$

Addition of calcium acetate into marennine crude extract containing an increasing amount of disodium phosphate resulted in an improved gelation yield up to a Ca/P molar ratio of 2, after which further phosphate addition resulted in a slight decrease in yield (fig. S14). The reaction occurring between calcium and phosphate is evidenced by the pH variation, as it decreases down to 5.6 then begin to rise upon total calcium consumption. The ideal phosphate concentration is described by Eq. (3).

$$[\text{HPO}_4^{2-}] = A_{\max} [\text{AU}] \cdot l [\text{cm}] \cdot 15 \left[ \text{mM} \cdot (\text{AU} \cdot \text{cm})^{-1} \right] \quad (3)$$

### 3.2.2. Dissolution (gel-sol transition)

Complete dissolution of the hydrogel was achieved at 30  $\text{mM}\cdot\text{AU}^{-1}$  for EDTA, with a recovery yield of 98 (2) %. For L-GLDA, twice this concentration was required to achieve the same effect and the yield was 102 (1) % (fig. S15). Eq. (4) outlines the relation between EDTA and the calcium input used in the gelation step (Eq. (2)), taking into account both input and output extract volumes, expressed as  $V_i$  and  $V_f$ , respectively.

$$[\text{EDTA}] = [\text{Ca}^{2+}] \cdot 1.5 \cdot (V_i/V_f) \quad (4)$$

## 3.3. Scaled extraction and purification

The scaled elution profile indicate that the CE is readily eluted, with most of the marennine recovered right after the dead volume. As such, 89 % desorption occurred between 300 and 700 mL of eluent, equivalent to 0.8–1.8  $\text{mL}\cdot\text{g}^{-1}$  of graphite. Fig. S17 shows the change in CE concentration as a function of eluent volume. Complete desorption was achieved at about 3.9  $\text{mL}\cdot\text{g}^{-1}$ .

### 3.3.1. Cation-induced spectral shift

Both cations induced a similar bathochromic shift, from 607 to 656 nm for sodium and 660 nm for magnesium. However, for sodium, this was accompanied by an hypochromic shift, whereas addition of magnesium resulted in a sharper band (figs. S18 and S19) and an hyperchromic shift, raising the relative absorbance to 115 % compared to desalted marennine (table S4).

### 3.3.2. Marennine extraction

The yields of marennine at each step are detailed in Table 1. Upon fractionation of marennine polymers, the 30–3 kDa retentate constituted the largest portion of the recovered marennine (48 %), followed by the 3–1 kDa retentate (26 %), the <1 kDa permeate (24 %) and the >30 kDa retentate (2 %). Only 29 % of marennine was recovered from the 1 kDa

**Table 1**

Summary of extracellular marennine yields obtained via the scaled batch extraction method.

Crude concentrate	$\lambda_{\max}$	Stepwise yield	Total yield	Dry mass / BW volume	
	(nm)	(%)	(%)	Experimental	Salinity-adjusted <sup>†</sup>
Blue water	659	–	100	–	–
SPE Crude extract	658	67	67	–	–
Gelation/dissolution	672	94	63	–	–
<b>Molecular weight</b>	<b>nm</b>	<b>%</b>	<b>%</b>	<b>mg·L<sup>-1</sup></b>	<b>mg·L<sup>-1</sup></b>
> 30 kDa	607	1 <sup>a</sup>	1 <sup>a</sup>	0.8	0.6
30–3 kDa	606	45 <sup>a</sup>	28 <sup>a</sup>	2.3	1.8
3–1 kDa	603	24 <sup>a</sup>	15 <sup>a</sup>	0.9	0.7
< 1 kDa (permeate)	673	22	14	–	–
Σ	–	93	58	4.0	3.1
<b>Molecular weight</b>	<b>nm</b>	<b>%</b>	<b>%</b>	<b>mg·L<sup>-1</sup></b>	<b>mg·L<sup>-1</sup></b>
<1 kDa (second SPE)	652	29	4	0.7	0.5

<sup>a</sup> Adjusted for hypochromic shift effect of desalination on the chromophore absorbance. Yield values were multiplied by 115 %.

<sup>†</sup> Adjusted for approximate salt residues based on measured electrical conductivity.

end-permeate, but its salinity was successfully decreased by the second SPE. However, this fraction still contains non-marennine EPS, which emits a distinctive, sweet odor. A total yield of 43 % was achieved for the main retentates, between 1 and 30 kDa, with the main loss occurring at the SPE step (–33 %).

### 3.3.3. Mass absorptivity

The two main marennine fractions, namely the 30–3 and 3–1 kDa retentates, had good to excellent mass absorptivity ( $\epsilon_m$ ), with values of 9.2 (0.1) and 13.4 (0.6) L·cm<sup>-1</sup>·g<sup>-1</sup>, respectively. According to their estimated salinity, their absorptivity might reach up to 11.8 and 17.8 L·cm<sup>-1</sup>·g<sup>-1</sup> following extensive desalination. While the high molecular weight retentate (> 30 kDa) accounts for nearly 20 % of total marennine dry mass (Table 1), it contains very little chromophore in comparison to other fractions. Mass absorptivity results are shown in Table 2.

### 3.3.4. EPS extraction and characterization

Among both EPS extraction methods, the lipophobic fractions had the highest sulfation degree compared to their methanol-soluble counterpart (table S6). Additionally, EPS obtained from the sequential SPE technique were distinctly darker and had a higher sulfation degree than EPS extracted from the gelation supernatant. Interestingly, among all samples, MMW marennine had the highest binding affinity after fucoidan. Lipophobic fractions represent over 60 % of the mass recovered in

**Table 2**

Mass absorptivity ( $\epsilon_m$ ) at 22 °C in sodium phosphate buffer (10 mM, pH 8).

Marennine molecular weight	$\lambda_{\max}$ (nm)	Experimental (L·cm <sup>-1</sup> ·g <sup>-1</sup> )	Salinity-adjusted <sup>a</sup> (L·cm <sup>-1</sup> ·g <sup>-1</sup> )
>30 kDa	665 (4)	0.4 (0.0)	0.6 (0.0)
30–3 kDa	670 (2)	9.2 (0.1)	11.8 (0.1)
3–1 kDa	668 (1)	13.4 (0.6)	17.8 (0.8)
<1 kDa	661 (1)	4.1 (0.2)	6.1 (0.4)

<sup>a</sup> Adjusted for approximate salt residues based on measured electrical conductivity.

the gelation supernatant and nearly all of the EPS extract obtained from the sequential BW extraction, reaching up to 85 % of the total extract content (table S5).

The ATR-FTIR spectra of the four EPS samples displayed many similarities with the fucoidan standard, including bands ascribed to sulfur atoms (table S7), and comprised all expected functional group characteristics of polysaccharides, such as a broad  $\nu(\text{O—H})$  at 3500–3000 cm<sup>-1</sup>, sharp  $\nu(\text{C—H})$  at 3000–2800 cm<sup>-1</sup>, strong and weak  $\nu(\text{COO}^-)$  near 1630–1600 and 1400 cm<sup>-1</sup>, weak  $\delta(\text{C—H})$  at 1380 cm<sup>-1</sup> and strong carbohydrates fingerprint bands between 1280 and 900 cm<sup>-1</sup> [22]. Detailed spectra can be found in figs. S20–S23.

## 4. Discussion

### 4.1. Solid-phase extraction improvements

Table 3 outline the major improvements achieved from the previous study [17], including the replacement of both the mobile and stationary phases, the introduction of a selective gelation technique and several steps contraction for an overall simplified SPE method. The sp<sup>2</sup> dominant structure of graphite is best suited for a typical reversed-phase chromatography behavior, and although its adsorption capacity is lower, graphite is widely available and inexpensive compared to specialty products such as GCB. Lastly, this smooth process avoids extreme pH exposure by eliminating the pre-elution step that involves TFA. As a result, the pH remains nearly constant at around 8 from the cultivation [23] up to the gelation step, where it varies from approximately 9 to 6.

**Table 3**

Summary of key improvements compared to the previous method described in Bélanger et al. [17].

	Previous method	Improved method
<b>Stationary phase</b>	Supelco Envicarb (GCB)	Mineral graphite (≥99% C)
Conditioning	Ethanol	–
Pre-treatment	Sodium metabisulfite (60 mM)	–
<b>Pre-elution steps</b>		
Desalting	Aqueous rinse	–
Water removal	Ethanol	–
<b>Coproduct extraction</b>	DCM:Methanol, TFA (6:4, 0.2 %, v/v)	–
DCM removal	Ethanol	–
pH equilibration	Sodium phosphate (100 mM)	–
<b>Mobile phase</b>	Buffer/Ethyl lactate	Water/2-Butanone
Solvent properties	Polar protic (acidic), bp. 154 °C	Polar aprotic (neutral), bp. 80 °C
Concentration (v/v)	35 %	20 %
Reducing agent	Sodium sulfite (5 mM)	–
Buffering	Sodium phosphate (100 mM)	–
<b>Precipitation</b>	Ethanol (80 %, v/v)	Disodium phosphate (15 mM·A <sub>max</sub> <sup>-1</sup> ) Calcium acetate (20 mM·A <sub>max</sub> <sup>-1</sup> )
<b>Resolubilization</b>	Water	EDTA (pH 8, 30 mM·A <sub>max</sub> <sup>-1</sup> )

#### 4.1.1. Stationary phase

As described in Muzyka et al. [21], Raman spectroscopy was used to evaluate the presence of heteroatoms on carbonaceous compounds. As such, comparing GCB and graphite reveals a clear distinction in their structure, with GCB exhibiting more oxygen groups (table S3), which are susceptible to cause ionic interactions [18]. This relation between  $sp^3$  defects on carbonaceous materials and ionic interactions is supported by the reduction experiment (fig. S3), as graphite yielded no significant differences between the groups, whereas GCB yield was greatly enhanced by the usage of sodium sulfite and metabisulfite. Lower GCB yields indicates a “capping” effect, suggesting that some ionized groups were not fully reduced, leading to persistent adsorption and yield loss even in the presence of reducing agents. Presumably, this effect could be intensified with an unsaturated sorbent. The lack of ionic interactions in high carbon containing graphite is thus ideal for marennine extraction, as reductants are not required, resulting in fewer inputs, simpler purification and gentler extraction. Both –325 and –100 mesh graphite flakes showed similar levels of adsorption and desorption capabilities, with the former exhibiting slightly superior performance due to its increased carbon content and contact surface. Conversely, the inferior yield of +50 mesh graphite is likely attributed to its lower surface area combined with higher oxygen content, thereby rendering it ineffective for marennine extraction. Furthermore, the use of the Raman  $I_D/I_G$  ratio revealed a strong correlation with SPE CE yields (Fig. 5), which upon validation could provide an efficient screening method for the evaluation of new carbonaceous sorbents for marennine extraction.

The progressive inversion of the yield to waste ratio during successive extractions suggests a build-up of organic compounds onto graphite, resulting in a decline of its adsorption capability (fig. S4). According to North et al. [24], most organic compounds decompose at temperatures above 300 °C, effectively stripping hydrogen and other noncarbon elements from carbon chains and rings. This may explain the improved adsorption capacity and increasing yield to waste ratio of heat-treated graphite compared to its pristine counterpart. Exposing graphite to 400 °C successfully reset and even enhanced its adsorption capabilities, although it also slightly reduce CE yield compared to pristine graphite. Regeneration temperature was limited to 400 °C to prevent adverse oxidation reactions, as graphite reactivity increases with temperature and readily oxidizes with water and oxygen near 450 °C [25]. Although the heat treatment duration was done in excess, according to thermogravimetric analysis (fig. S6), an exposure time of <1 h would likely produce the same effect. Additionally, stationary phase conditioning and prevention of drying between steps had no significant effect on yields (fig. S2). Consequently, these steps were discarded.

#### 4.1.2. Mobile phase

Choice of solvents can have a major impact on cost, safety, health hazards and environmental performance of a chemical process, thus making a careful selection in the early phases of the process design crucial [26]. Replacement of ethyl lactate with 2-butanone in the mobile phase improved the extraction of marennine due to its aprotic, pH-neutral nature. 2-butanone is a volatile organic compound similar to acetone, commonly used as a solvent for paints and varnishes [27]. It has a low environmental impact as its mineralization in soil occur following a 2 to 4 week acclimation period [28]. Likewise, McCay et al. [29] reported that butanone presents overall little hazards to the aquatic biota. While large amounts can affect the soil ecosystems, given its high volatility butanone is rarely residual in soils and its environmental fate is expected to mainly occur in the atmosphere [27,30], with a lifetime of about 10 days [31]. It is generally considered safe to handle, with low toxicity [32]. The EHS assessment, used to evaluate hazardousness of solvents, revealed a similar profile to ethanol, despite its irritant properties which are closer to isopropanol [26]. Butanone is a suitable candidate as it is less toxic than acetonitrile, provides a better yield than acetone and is stabler than ethyl lactate. It is also readily accessible and can be sourced from renewable feedstocks via the dehydration of 2,3-

butanediol [33].

Yields using butanone in the mobile phase increased with concentration, reaching 60 % at near half the volume of ethyl lactate (20 % vs 35 %, v/v) [17]. The boiling point of butanone (80 °C) is also twice lower than ethyl lactate (154 °C) [34,35], improving energy efficiency for solvent recycling and recovery of coproducts in BW (Fig. 1). Buffering was found unnecessary due to the aprotic nature of butanone. As indicated by Hennion [18], backflush desorption resulted in a marennine CE yield increase, reaching up to 84 (2) % (fig. S2).

#### 4.2. Reversible ionotropic gelation

In replacement of the SPE pre-elution wash and anti-solvent precipitation [17], marennine pigment is gellified by in situ synthesis of calcium phosphate salts, an approach comparable to the gelification of alginate and other polysaccharides [36]. For this purpose, calcium acetate is used as a nontoxic source of  $Ca^{2+}$ , biosourceable from bivalves and eggshells [37,38], and recognized as a food safe additive [39]. Being highly soluble in water (0.26  $g \cdot g^{-1}$ , 25 °C) [40], it provides an advantageous compromise between the solubility of calcium chloride and the safety of calcium sulfate.

##### 4.2.1. Gelation (sol-gel transition)

Adding  $HPO_4^{2-}$  and  $Ca^{2+}$  ions to the hydroorganic CE resulted in the formation of insoluble salts that coordinates with marennine and drives it out of the solution, greatly enhancing gelation compared to calcium alone (fig. S13). Optimization of the calcium to phosphate ratio revealed that the supernatant pH decreases progressively as the concentration of disodium phosphate increases, until a Ca/P ratio of 2 is reached. Beyond this point, further phosphate addition begins to raise the pH, indicating complete calcium consumption at a Ca/P ratio between 1.5 and 2 (fig. S14). This, along with the release of  $H^+$  upon reaction of both ions, refutes the possibility of a simple calcium phosphate salt such as  $CaHPO_4$ . Raman and FTIR analysis of the isolated salts suggest the formation of a compound similar to hydroxyapatite ( $Ca_5(PO_4)_3(OH)$ ), yet different as the bands related to the OH group are missing from both spectra (fig. S16). Lastly, the slight increase of the gelation effectiveness relative to marennine concentration indicates possible crosslinking and agglomeration among polymer chains.

##### 4.2.2. Dissolution (gel-sol transition)

Following gelation, a water-insoluble form of marennine (EMn-CaP) is obtained, which can be further purified using solid-liquid extractions. Its dissolution is then achieved by substituting calcium ions with protons ( $H^+$ ), divalent cations ( $Mg^{2+}$ ), or through a chelation reaction. As strong acids affect marennine's ionization state, chelating agents were the most efficient and gentle approach to efficiently put marennine back in solution while preserving its molecular integrity.

Chelators are polydentate molecules capable of forming coordination bonds with metal ions to create stable complexes, facilitating cation isolation and removal [41]. Among aminopolycarboxylic acids, EDTA is a widely used and effective chelating agent, with a 1:1 ratio for  $Ca^{2+}$  capture [42]. However, EDTA is highly stable and thus not readily biodegradable [41,43]. An alternative is L-GLDA, which exhibits the required features for high calcium binding activity [41,43]. Unlike EDTA, it is mostly biosourced from glutamate or glutamic acid and is readily biodegradable according to OECD test guidelines, both uncomplexed and as a calcium chelate [41,44]. However, in practice EDTA was twice as effective for EMn-CaP dissolution, hence its use was considered favorable from an atom economy perspective.

#### 4.3. Scaled process and polymers fractionation

The elution profile (fig. S17) shows that most of the marennine is eluted just after the dead volume. Some tailing occurred, which might be related to marennine's polydispersity. Although the batch extraction

system was chosen for simplicity, the yield loss at this step is the highest for the entire process, so further optimization is needed. While more involving, a pressurized column could improve the yield, as the yield at near-saturation and the backflush experiments (Figs. 5, S2) suggest that, in ideal conditions, about 85 % can be achieved for the SPE step.

The relative absorbance of the four fractions isolated by cascade diafiltration (Table 1) revealed that the composition of marennine was 2 % HMW (>30 kDa), 48 % MMW (30–3 kDa), 26 % LMW (3–1 kDa) and 24 % VLMW (<1 kDa), with a high proportion of dry mass from the HMW fraction, albeit with a marginal chromophore content. Despite diafiltration being a theoretically lossless step, a discrepancy was found between the total yield at the edetate dissolution step (63 %) and the sum of the molecular weight fractions obtained by cascade diafiltration (52 %). As such, it was observed that upon desalination, an hypochromic shift occurred, where the chromophore's visible  $\lambda_{\max}$  moved from 663 (8) to 605 (2) nm, manifesting as a change from green to a deep blue color. This effect was accompanied by a hypochromic shift, biasing the yield downwards. Magnesium ions were found to cause this reversible effect, which upon addition increases the absorbance by a factor of 1.15 (table S4). The mass absorptivity of the 30–3 kDa retentate reached  $9.2 \text{ L}\cdot\text{cm}^{-1}\cdot\text{g}^{-1}$ , equivalent to 76 % of the purity reported by Pouvreau et al. [2] for that range of molecular weight ( $12.1 \text{ L}\cdot\text{cm}^{-1}\cdot\text{g}^{-1}$ ), whereas the 3–1 kDa fraction outpassed that value and attained the highest  $\epsilon_m$  reported to date, at  $13.4 \text{ L}\cdot\text{cm}^{-1}\cdot\text{g}^{-1}$ . It is expected that salt residues play an important role in these results.

While emphasis was put on the purification and fractionation of marennine polymers to demonstrate process versatility and provide insights into BW composition, diafiltration can be a time-prohibitive step, particularly for the concentration of large volume of 3 kDa permeate onto the 1 kDa membrane, which can take several days. To address this, two alternatives are proposed to achieve similar marennine extracts (Fig. 6). Among those, the diafiltration pathway starts with desalination via continuous diafiltration on a 1 kDa membrane, which is slow but can be left unattended once equilibrium is reached. The retentate is then moved onto a fast-flowing 30 kDa membrane to remove particulate matter and high molecular weight compounds. This approach minimize losses and improves time efficiency, while preserving fine control over the desalination process. It is suitable for most use cases where high purity is desirable, yet separation of marennine fractions are not required, providing a straightforward, scalable alternative to the previously used combination of ionic chromatography and dialysis. The second SPE pathway, though providing lower yield and quality, offers a whole marennine extract, is low cost, and is faster since it avoids the need for diafiltration. Still, for higher yield and quality it is recommended to use the diafiltration pathway when possible, along with

optional extraction of the VLMW marennine from the 1 kDa permeate, as shown in Fig. 3.

As first shown in our preliminary study [17], the presence of sulfated polysaccharides in BW was again confirmed. To this end, two complementary methods were employed, one of which also serves as a recycling step for the SPE eluent (Fig. 4). The results of both techniques revealed related, yet different compounds, which all tested positive for the presence of sulfate via the toluidine blue experiment (table S6) and displayed ATR-FTIR spectra consistent with fucoidan extracted from *Fucus vesiculosus* (table S7). A sequential BW extraction was performed as a proof of concept to demonstrate the untapped potential for further valorization of spent BW following marennine extraction. Optimization of this step could provide a large amount of sulfated polysaccharides with low effort, as the extract was cleaner and required less workup compared to the extraction from the gelation supernatant. Additionally, results from the toluidine blue experiment showed that these EPS have a higher sulfation degree, which could result in increased bioactivity [45]. Surprisingly, the medium MW fraction of marennine (30–3 kDa retentate) reacted strongly with the toluidine blue, reaching 70 % of fucoidan effectiveness. As it is assumed that the low pH has protonated carboxylate groups, it appears that sulfates are present. Therefore, additional research should be conducted to investigate a possible connection between sulfation and marennine bioactivity.

## 5. Conclusion

Marennine's importance lies in its significant prophylactic properties and its effectiveness in inhibiting bacterial pathogens such as *Vibrio*. While many attempts were made to achieve small-scale extractions, there is a need for a scalable preparative method that efficiently isolates marennine while preserving its stability, using low-cost and green inputs. Therefore, thorough improvements to our solid-phase extraction method were achieved by replacing the mobile and stationary phases, both of which are reusable, adding to the cost effectiveness and sustainability of the process. The mobile phase is water-based and employed 2-butanone as an aprotic, low-toxicity organic modifier. Natural graphite flakes were found to be best suited as a stationary phase over GCB, due to their lower oxygen content and lack of ionic interactions. Following SPE, marennine was purified from co-extracted EPS through selective gelation using disodium phosphate and calcium acetate, providing a gentle approach to isolate the polymers from the hydroorganic crude extract with minimal pH variation. Aqueous marennine was then restored with chelator-assisted gel dissolution using EDTA, followed by further purification or desalination by means of diafiltration or a second SPE. The scaled process showed promising

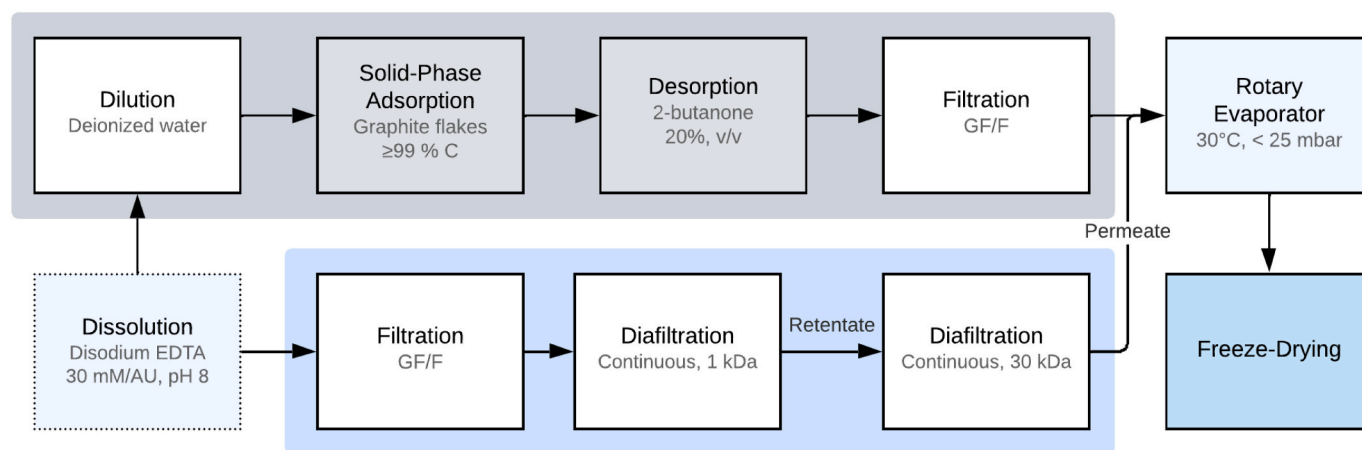


Fig. 6. As a complement to Fig. 1, this schematic illustration proposes two alternative routes for the desalination and purification of marennine extracts containing calcium-EDTA chelates. The diafiltration pathway is shown in blue, and the second SPE pathway in gray. (For interpretation of the references to color in this figure legend, the reader is referred to the web version of this article.)

marennine yields and purity, yet allowing for potential improvement using a pressurized SPE column in replacement of the batch extraction system. In addition to the demonstrated fractionation of marennine polymers among several molecular weight groups, the isolation of four sulfated polysaccharides suggests great prospects beyond marennine production for further valorization of *Haslea ostrearia*'s culture supernatant. Hence, our successful development of a scalable, eco-friendly method for extracting marennine polymers in mild conditions marks a significant step forward in developing sustainable and efficient marennine extraction processes, and for the valorization of *Haslea* culture as a whole.

### CRedit authorship contribution statement

**William Bélanger:** Writing – review & editing, Writing – original draft, Visualization, Software, Methodology, Investigation, Formal analysis, Data curation. **Richard Saint-Louis:** Writing – review & editing, Supervision, Resources. **Bertrand Genard:** Resources. **Jean-Sébastien Deschênes:** Writing – review & editing, Resources. **Réjean Tremblay:** Writing – review & editing, Supervision, Resources, Project administration, Funding acquisition.

### Funding

This work was supported by the Ressource Aquatiques Québec Research Network [Fonds de Recherche du Québec - Nature et Technologies, no. 2014-RS-171172] and the Québec Ministry of Economy and Innovation Québec [Project PADS-56972].

### Declaration of competing interest

The authors declare that they have no known competing financial interests or personal relationships that could have appeared to influence the work reported in this paper.

### Acknowledgments

The authors would like to thank Alexandre Coulombe, Jonathan Coudé, Marie-Ève Anglehart, Nathalie Gauthier, Steeven Ouellet and Ressources Aquatiques Québec (RAQ) for their technical assistance.

### Appendix A. Supplementary data

Supplementary data to this article can be found online at <https://doi.org/10.1016/j.algal.2024.103879>.

### Data availability

Data will be made available on request.

### References

- Nellie Francezon, Mickaël Herbaut, Jean-François Bardeau, Charles Cougnon, William Bélanger, Réjean Tremblay, Boris Jacquette, Jens Dittmer, Jean-Bernard Pouvreau, Jean-Luc Mouget, et al., Electrochromic properties and electrochemical behavior of marennine, a bioactive blue-green pigment produced by the marine diatom *haslea ostrearia*, *Mar. Drugs* 19 (4) (2021) 231.
- Jean-Bernard Pouvreau, Michele Moranaïs, Fabrice Fleury, Philippe Rosa, Laurent Thion, Blanche Cahing, Franck Zal, Joël Fleurence, Pierre Pondaven, Preliminary characterisation of the blue-green pigment "marennine" from the marine tychopelagic diatom *haslea ostrearia* (gaillon/bory) simonsen, *J. Appl. Phycol.* 18 (6) (2006) 757–767.
- Romain Gastineau, François Turcotte, Jean-Bernard Pouvreau, Michèle Moranaïs, Joël Fleurence, Eko Windarto, Fiddy Semba Prasetya, Sulastri Arsad, Pascal Jaouen, et al., Marennine, promising blue pigments from a widespread *haslea* diatom species complex, *Mar. Drugs* 12 (6) (2014) 3161–3189.
- Romain Gastineau, Gert Hansen, Michel Poulin, Claude Lemieux, Monique Turmel, Jean-François Bardeau, Vincent Leignel, Yann Hardivillier, Michèle Moranaïs, Joël Fleurence, et al., *Haslea silbo*, a novel cosmopolitan species of blue diatoms, *Biology* 10 (4) (2021) 328.
- Zeineb Bouhlel, Alexandre A. Arnold, Jean-Sébastien Deschênes, Jean-Luc Mouget, Dror E. Warschawski, Réjean Tremblay, Isabelle Marcotte, Investigating the action of the microalgal pigment marennine on *vibrio splendidus* by in vivo 2h and 31p solid-state nmr, *Biochim. Biophys. Acta (BBA)-Biomembr.* 1863 (9) (2021) 183642.
- Jordan C.-T. Latour, Sarah-Béatrice Bernier, Kim Doiron, Réjean Tremblay, Karine Lemarchand, Effect of marennine on the rearing medium and microbiota of *mytilus edulis* larvae and its protective effect after exposure to the pathogenic *vibrio splendidus*, *J. Appl. Aquac.* (2023) 1–21.
- Fiddy S. Prasetya, Sunarto Sunarto, Eri Bachtiar, Mochamad U.K. Agung, Bram Nathanael, Ardian C. Pambudi, Ajeng D. Lestari, Sri Astuty, Jean-Luc Mouget, Effect of the blue pigment produced by the tropical diatom *haslea nansantara* on marine organisms from different trophic levels and its bioactivity, *Aquac. Rep.* 17 (2020) 100389.
- François Turcotte, Jean-Luc Mouget, Bertrand Genard, Karine Lemarchand, Jean-Sébastien Deschênes, Réjean Tremblay, Prophylactic effect of *haslea ostrearia* culture supernatant containing the pigment marennine to stabilize bivalve hatchery production, *Aquat. Living Resour.* 29 (4) (2016) 401.
- N. Elodie Pedron, J.-L. Mouget Gargouch, R. Tremblay, J.-S. Deschênes, A. Massé, O. Gonçalves, Hybrid photobioreactor operation for the intensified production of *haslea ostrearia* and marennine in function of strain variability, *Algal Research* 75 (2023) 103285.
- Fiddy S. Prasetya, Martin Foret, Jean-Sébastien Deschênes, Romain Gastineau, Jean-Luc Mouget, Réjean Tremblay, Semi-continuous system for benthic diatom cultivation and marennine production, *Algal Res.* 62 (2022) 102633.
- R. Nghiem Xuan, I. Safitri, J.L. Mouget, V. Jeremy Pruvost, Turpin, and P Jaouen., Design of an artificial culture medium to optimize *haslea ostrearia* biomass and marennine production, *Algal Res.* 45 (2020) 101653.
- Nesrine Gargouch, Raphaëlle Touchard, Hélène Marec, Jean Luc Mouget, Jérémy Pruvost, Anthony Massé, Submerged membrane photobioreactor for the cultivation of *haslea ostrearia* and the continuous extraction of extracellular marennine, *Bioresour. Technol.* 350 (2022) 126922.
- Nathalie Rossignol, Pascal Jaouen, Jean-Michel Robert, Francis Quéméneur, Production of exocellular pigment by the marine diatom *haslea ostrearia* simonsen in a photobioreactor equipped with immersed ultrafiltration membranes, *Bioresour. Technol.* 73 (2) (2000) 197–200.
- Ilhem Zebiri, Boris Jacquette, Nellie Francezon, Mickaël Herbaut, Amina Latigui, Sullivan Bricaud, Réjean Tremblay, Pamela Pasetto, Jean-Luc Mouget, Jens Dittmer, The polysaccharidic nature of the skeleton of marennine as determined by nmr spectroscopy, *Mar. Drugs* 21 (1) (2023) 42.
- Jean-Bernard Pouvreau, Michele Moranaïs, Guillaume Massé, Philippe Rosa, Jean-Michel Robert, Joël Fleurence, Pierre Pondaven, Purification of the blue-green pigment "marennine" from the marine tychopelagic diatom *haslea ostrearia* (gaillon/bory) simonsen, *J. Appl. Phycol.* 18 (6) (2006) 769–781.
- Jörg Thömmes, Mark Etzel, Alternatives to chromatographic separations, *Biotechnol. Prog.* 23 (1) (2007) 42–45.
- William Bélanger, Alexandre A. Arnold, François Turcotte, Richard Saint-Louis, Jean-Sébastien Deschênes, Bertrand Genard, Isabelle Marcotte, Réjean Tremblay, Extraction improvement of the bioactive blue-green pigment "marennine" from diatom *haslea ostrearia*'s blue water: a solid-phase method based on graphitic matrices, *Mar. Drugs* 18(12):653 (2020).
- Marie-Claire Hennion, Graphitized carbons for solid-phase extraction, *J. Chromatogr. A* 885 (1–2) (2000) 73–95.
- Dennis L. Corwin, Kevin Yemoto, Salinity: electrical conductivity and total dissolved solids, *Soil Sci. Soc. Am. J.* 84 (5) (2020) 1442–1461.
- Thomas Hahn, Mariya Schulz, Ralf Stadtmüller, Ahmed Zayed, Kai Muffler, Siegmund Lang, Roland Ulber, Cationic dye for the specific determination of sulfated polysaccharides, *Anal. Lett.* 49 (12) (2016) 1948–1962.
- Roksana Muzyka, Sabina Drewniak, Tadeusz Pustelny, Maciej Chrusabik, Grazyna Gryglewicz, Characterization of graphite oxide and reduced graphene oxide obtained from different graphite precursors and oxidized by different methods using raman spectroscopy, *Materials* 11 (7) (2018) 1050.
- Qingbin Guo, Lianzhong Ai, Steve Cui, Methodology for Structural Analysis of Polysaccharides, Springer, 2019.
- R. Nghiem Xuan, J.L. Mouget, V. Turpin, P. Jaouen, Jeremy Pruvost, Optimization of the growth and marennine production by the diatom *haslea ostrearia* in photobioreactor, *Algal Res.* 55 (2021) 102251.
- Gerald R. North, John A. Pyle, Fuqing Zhang, *Encyclopedia of Atmospheric Sciences* vol. 1, Elsevier, 2014 (ISBN 9780123822253.).
- Hugh O. Pierson, *Handbook of Carbon, Graphite, Diamonds and Fullerenes: Processing, Properties and Applications*, Noyes Publication, 1993 (ISBN 0815513399.).
- Paweł Wiczling, Michal J. Markuszewski, Roman Kaliszan, Determination of  $pK_a$  by pH gradient reversed-phase HPLC, *Anal. Chem.* 76 (11) (2004) 3069–3077.
- Yooeun Chae, Rongxue Cui, Jongmin Moon, Youn-Joo An, Ecological hazard assessment of methyl ethyl ketone using the species sensitivity distribution approach in a soil ecosystem, *J. Hazard. Mater.* 360 (2018) 490–497.
- Joseph M. Sulflita, Melanie R. Mormile, Anaerobic biodegradation of known and potential gasoline oxygenates in the terrestrial subsurface, *Environ. Sci. Technol.* 27 (5) (1993) 976–978.
- Deborah P. French McCay, Nicole Whittier, Matthew Ward, Claudia Santos, Spill hazard evaluation for chemicals shipped in bulk using modeling, *Environ. Model. Software* 21 (2) (2006) 156–169.
- Chang Ji, Emily M. Evans, Using an internal standard method to determine Henry's law constants, *Environ. Toxicol. Chem.* 26 (2) (2007) 231–236.
- Roger Atkinson, Atmospheric chemistry of vocs and nox, *Atmos. Environ.* 34 (12–14) (2000) 2063–2101.

- [32] Fergal P. Byrne, Saimeng Jin, Giulia Paggiola, Tabitha H.M. Petchey, James H. Clark, Thomas J. Farmer, Andrew J. Hunt, C. Robert McElroy, James Sherwood, Tools and techniques for solvent selection: green solvent selection guides, *Sustain. Chem. Process.* 4 (1) (2016) 1–24.
- [33] Daesung Song, Yeong-Gak Yoon, Chul-Jin Lee, Conceptual design for the recovery of 1, 3-butadiene and methyl ethyl ketone via a 2, 3-butanediol-dehydration process, *Chem. Eng. Res. Des.* 123 (2017) 268–276.
- [34] Carla S.M. Pereira, Viviana M.T.M. Silva, Alfrio E. Rodrigues, Ethyl lactate as a solvent: properties, applications and production processes—a review, *Green Chem.* 13 (10) (2011) 2658–2671.
- [35] Ian Smallwood, *Handbook of Organic Solvent Properties*, Butterworth-Heinemann, 2012.
- [36] Pornsak Sriamornsak, Ross A. Kennedy, Swelling and diffusion studies of calcium polysaccharide gels intended for film coating, *Int. J. Pharm.* 358 (1–2) (2008) 205–213.
- [37] Montree Thongkam, Jinnaput Saelim, Banjong Boonchom, Somkiat Seesanon, Kittichai Chaiseeda, Nongnuch Laohavisuti, Kanokpon Bunya-atichart, Wimonmat Boonmee, Duangkamol Taemchuay, Simple and rapid synthesis of calcium acetate from scallop shells to reduce environmental issues, *Adsorpt. Sci. Technol.* 2021 (2021).
- [38] Yutong Yao, Jing Zhang, Run Zhang, Yueru Shi, Peipei An, Hu Xin, Youzhong Wan, Optimization of preparation of calcium acetate from eggshell by response surface methodology (rsm), *Food Sci. Technol.* 42 (2022).
- [39] Anastasiya Demydova, Fedor F. Gladkiy, Olena F. Aksonova, Svitlana M. Molchenko, A study of the influence of calcium acetate on the process of sunflower oil degumming, *J. Chem. Technol.* 29 (2) (2021) 301–311.
- [40] Dale L. Perry, *Handbook of Inorganic Compounds*, CRC press, 2016.
- [41] Tariq Almubarak, Jun Hong Ng, Raja Ramanathan, Hisham A. Nasr-El-Din, From initial treatment design to final disposal of chelating agents: a review of corrosion and degradation mechanisms, *RSC Adv.* 12 (3) (2022) 1813–1833.
- [42] Matteo Cibinel, Giorgia Pugliese, Davide Porrelli, Lucia Marsich, Vanni Lughì, Recycling alginate composites for thermal insulation, *Carbohydr. Polym.* 251 (2021) 116995.
- [43] Helena Hyvönen, et al., *Studies on Metal Complex Formation of Environmentally Friendly Aminopolycarboxylate Chelating Agents*, 2008.
- [44] Cornelis G. van Ginkel, Roy Geerts, Phuong D. Nguyen, *Biodegradation of L-Glutamatediacetate by Mixed Cultures and an Isolate*, ACS Publications, 2005.
- [45] Peili Shen, Zongmei Yin, Qu Guiyan, Chunxia Wang, Fucoidan and its health benefits, in: *Bioactive Seaweeds for Food Applications*, Elsevier, 2018, pp. 223–238.